https://doi.org/10.5194/tc-2022-185
Preprint. Discussion started: 4 October 2022

The Cryosphere Discussions
Open Access
EGU

Attributing near-surface atmospheric trends in the Fram Strait region to regional sea ice conditions

Amelie U. Schmitt[1] and Christof Lüpkes[2]

[1]Meteorological Institute, Center for Earth System Research and Sustainability (CEN), Universität Hamburg, Hamburg, Germany
[2]Alfred Wegener Institute, Helmholtz Centre for Polar and Marine Research, Bremerhaven, Germany

Correspondence: Amelie Schmitt (amelie.schmitt@uni-hamburg.de), Christof Lüpkes (christof.luepkes@awi.de)

Abstract. Arctic sea ice has declined in all seasons accompanied by a rapid atmospheric warming. Here, the focus lies on the wider Fram Strait region where the connection between trends in observed near-surface variables (temperature, humidity, wind speed) and local sea ice conditions are analyzed. Reanalysis data from ERA5 and MERRA-2 for the winters 1992 to 2022 are used for the analyses. To disentangle the impact of the upstream sea ice conditions from other factors influencing atmospheric conditions, separate calculations are applied for on-ice and off-ice flow. During off-ice flow, temperatures increased by more than 9 K within 31 years in the Western Nansen Basin (WNB) and by about 5 K in the Greenland Sea region (GRL). Humidity also increased significantly in both regions but with smaller trends in the GRL region. Trends for wind speed were mostly not significant.

Corresponding trends of winter sea ice concentrations based on SSM/I-ASI data show a decrease of -10 % dec^{-1} in the WNB region with especially large open water areas in 2022. There are clear hints that sea ice variability in the GRL region is strongly influenced by the presence of the Odden ice tongue and thus it shows a decrease of -4.7 % dec^{-1}. For off-ice flow, upstream sea ice conditions in the Fram Strait region influence atmospheric temperatures and humidity up to 500 km downstream of the ice edge. Up to two thirds of the observed temperature variability in both regions can be explained by upstream sea ice variability, which is about 10 % more than for all other wind directions.

1 Introduction

In the last decades the Arctic climate changed rapidly with a much stronger increase of atmospheric temperatures than in mid latitudes. This phenomenon, called the Arctic Amplification, has been described in many articles (e.g. Cohen et al., 2014; Graversen et al., 2008). Temperature increase went along with an unprecedented decrease of sea ice extent (SIE) (Stroeve et al., 2012, 2014). Shu et al. (2020) analyzed different satellite datasets from 1979 to 2014 and found that SIE decreased in all seasons with trends of about -0.82 and -0.35 million km^2 per decade in September and March, respectively. Stroeve and Notz (2018) and Onarheim et al. (2018) found that the strength of the trend highly depends on region where the largest decrease of SIE was located in the Beaufort and East Siberian Seas in September and in the Barents and Greenland seas in March.

In this study, we focus on winter conditions in the Fram Strait region, which contains parts of the Greenland and Barents seas. Our aim is to identify ongoing changes of regional atmospheric near-surface conditions and their relations to observed changes

https://doi.org/10.5194/tc-2022-185
Preprint. Discussion started: 4 October 2022

in sea ice cover. Various studies have already addressed the close connection of sea ice loss with processes in the atmosphere and ocean. For example, sea ice changes can influence atmospheric variables such as the regional pressure field (Schneider et al., 2021) or cloud radiative forcing (Stapf et al., 2020). Decreasing sea ice concentration also impacts atmospheric temperature, wind and density stratification in the atmospheric boundary layer (e.g. Lüpkes et al., 2008; Tetzlaff et al., 2015; Chechin et al., 2019; Michaelis et al., 2021; Wang et al., 2019).

One area of specific interest for regional studies has been the Greenland Sea. Moore et al. (2015) showed that the wintertime retreat of sea ice in the Greenland and Iceland seas reduced the magnitude of air-sea fluxes by 20 % since 1979 with potential future implications for the Atlantic Meridional Overturning Circulation. Selyuzhenok et al. (2020) found a link between the decrease of sea ice volume in the Greenland Sea between 1979 and 2016 and an increase of the amount of upper-ocean heat content available for sea ice melt related to increased temperatures of the Atlantic Water inflow in this region. An interesting local phenomenon in this region is the so-called Odden ice tongue, which occurred regularly until the early 1990ies in the region influenced by the Jan Mayen current (Wadhams and Wilkinson, 1999). Comiso et al. (2001) showed that the extent of the Odden ice tongue between 1979 and 1998 was affected by surface winds and had a strong negative correlation with the monthly surface air temperature recorded at Jan Mayen island.

Several other studies also considered the region around Svalbard and proposed different mechanisms that could explain recent sea ice trends. Ivanov et al. (2012) concentrated on the role of Atlantic water inflow in shaping the ice conditions between Svalbard and Franz Joseph Land. They found that sea ice conditions around Svalbard substantially affect the temperature regime of the Spitsbergen archipelago, particularly in winter. They conclude that in the Atlantic Water inflow, heat flux from the ocean reduces the sea ice thickness and thus trends in the ocean currents around Svalbard could have a profound effect on Svalbard climate. Dahlke et al. (2020) analyzed the sea ice variability around Svalbard from 1980 to 2016 and found a different explanation for decreasing SIE in the northern fjords in winter in the last 15-20 years. They calculated lag correlations with a time shift of 1 month, which indicate that atmospheric warming leads the sea ice signal and not vice versa. Lundesgaard et al. (2021) considered the water inflow region north of Svalbard and state that the sea ice concentration in this region is influenced by many different factors including atmospheric and oceanic forcing. They find, e.g. that between 2012 and 2019, heat flux from the ocean could not explain the interannual variability in sea ice concentration but sea ice drift was playing a key role. Isaksen et al. (2016) relate the recent strong warming of Spitsbergen to variations in the large scale atmospheric circulation, air mass characteristics and sea ice concentration around Spitsbergen. They find a high correlation between the land-based surface air temperature and local and regional sea ice concentration and finally that the strong warming in recent decades over the Svalbard Archipelago is driven by higher sea surface temperature and sea ice decline.

In this study, we consider the connection between meteorological quantities and sea ice cover in two regions, which are the region north of Spitsbergen and the region along the eastern Greenland coast. The first one was in the center of two studies, one by Onarheim et al. (2014) and another one by Tetzlaff et al. (2014). Both showed a strong sea ice decline in the region of the Whalers Bay polynya at the northern coast of Spitsbergen. Onarheim et al. (2014) shows that in this region loss of sea ice concerns especially winter, while in the entire Arctic Ocean sea ice is shrinking mainly during summer. Tetzlaff et al. (2014)

https://doi.org/10.5194/tc-2022-185
Preprint. Discussion started: 4 October 2022

find a close connection with local atmospheric processes such as an unprecedented high value of the atmospheric convective boundary-layer height in cold-air outbreaks during spring 2013 caused by the northward shift of the ice edge.

Here, we analyze regional trends of near-surface air temperatures and - departing from previous studies - also of humidity and wind speed between January and March for the years 1992 to 2022. Our results are based on data from the ERA5 and MERRA-2 reanalyses, which have a high spatial resolution and are thus ideal for studying also smaller regional differences. We then aim to answer the following question: can we attribute the observed changes in atmospheric quantities to changes in sea ice cover? For this purpose, we calculate regional sea ice trends and corresponding correlation coefficients between sea ice and atmospheric conditions. To separate the impact of sea ice changes from other factors influencing atmospheric conditions (e.g. warm air intrusions), we separately analyze results for different wind directions. The idea behind this is that especially during off-ice flow (so-called cold air outbreaks) strong convection occurs over the open ocean, and the highest vertical fluxes of heat and humidity occur near the ice margins where they have a profound impact on processes in the atmospheric boundary layer. Tetzlaff et al. (2014) showed that a sea ice reduction caused an extension of the ocean region that is strongly influenced by cold air outbreaks and related atmospheric convection to the north of Svalbard in 2013. On the other hand, warm air intrusions transport warm and humid air masses northward, so that there are two competing mechanism related to on- and off-ice flow. Thus, comparing correlations for different wind direction sectors helps us to disentangle the complex interactions influencing near-surface atmospheric trends.

The used datasets and applied methods are described in Sect. 2. First, we analyze trends in meteorological variables (Sect. 3.1) and sea ice (Sect. 3.2) separately. This is followed by a correlation analysis in Sect. 3.3 and a discussion of the results and conclusions in Sect. 4.

2 Data and methods

2.1 Sea ice concentration

To analyze sea ice trends in the Fram Strait region we use the SSM/I-ASI sea ice concentration dataset provided by Ifremer. Sea ice concentration is derived from space-borne passive microwave measurements – namely brightness temperatures measured at the 85 GHz channel of the Special Sensor Microwave / Imager (SSM/I) and its successor, the Special Sensor Microwave / Imager Sounder (SSM/IS). The ARTIST Sea Ice (ASI) algorithm (Kaleschke et al., 2001; Spreen et al., 2008) is applied to compute sea ice concentration, followed by a 5-day median filter to reduce the weather impact (Kern et al., 2010). The data are provided on a polar-stereographic grid with a resolution of 12.5 km x 12.5 km. In this study, we use 31 years of winter data (January – March) from 1992 to 2022.

2.2 Reanalysis datasets

The fifth generation of the ECMWF atmospheric reanalysis (ERA5) provides hourly data with a horizontal resolution of 0.25° x 0.25° on 137 vertical levels (Hersbach et al., 2020). Here, we use air temperature, specific humidity and horizontal wind

https://doi.org/10.5194/tc-2022-185
Preprint. Discussion started: 4 October 2022

components from the lowest model level, which has an average height of about 9 m for this region and season. Data for the years 1992 to 2022 were downloaded from the Copernicus Climate Change Service (C3S) Climate Data Store (Hersbach et al., 2017).

Version 2 of the Modern-Era Retrospective analysis for Research and Applications (MERRA-2) provides hourly data on a 0.5°-latitude and 0.625°-longitude grid and on 72 vertical levels (Gelaro et al., 2017). Here, we use air temperature, specific humidity and horizontal wind components at 10 m height for the years 1992 to 2022 from the single level diagnostics dataset provided by Global Modeling and Assimilation Office (GMAO) (2015).

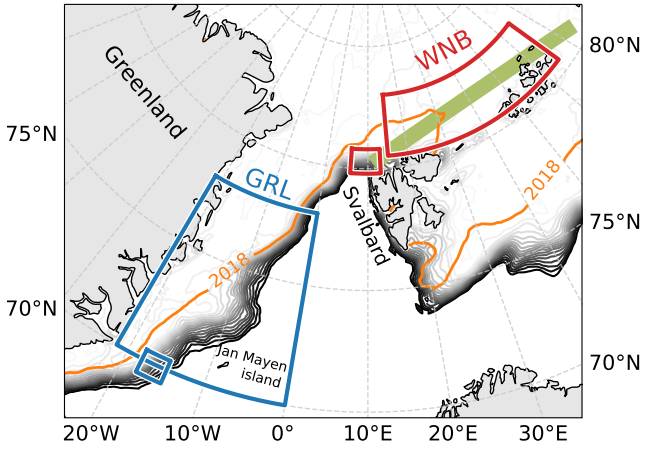

Figure 1. Overview map of the study region. January to March averages of the SSM/I-ASI sea ice concentration are displayed as grey contours from 15 % upward in 5%-steps for 1996 (a year with large SIE) and as orange 15 %-contour for 2018 (a year with small SIE). Large ICE boxes indicate the areas considered for trends of sea ice conditions and small ATM boxes indicate areas considered for atmospheric trends in the Greenland Sea (GRL, blue) and the Western Nansen Basin (WNB, red) regions, respectively. The green thick line indicates the path considered for WNB fetch calculations.

2.3 Study region and WNB fetch length

We selected two focus areas in the wider Fram Strait region (Fig. 1). The first one is located at the Western Nansen Basin (WNB) north-east of Svalbard - also called the Whaler's Bay polynya - which has been the study area in previous works by Ivanov et al. (2012), Onarheim et al. (2014) and Tetzlaff et al. (2014). The exact location of all boxes considered for trends in sea ice (ICE box) and atmospheric variables (ATM box) can be found in Tab. 1. The second focus area is located in the Greenland Sea (GRL) at the east coast of Greenland (Fig. 1). Our aim was to place the GRL ICE box in such a position that it covers the full extent of the Odden ice tongue, which is present in some of the considered years, and thus we chose the location of the box accordingly. This means, however, that the GRL ICE box contains much more open ocean regions than the WNB ICE box and thus the sea ice cover trends are expected to be smaller.

https://doi.org/10.5194/tc-2022-185
Preprint. Discussion started: 4 October 2022

We also study trends of atmospheric variables in a region influenced by the changing sea ice cover in the WNB and GRL regions. Besides focusing on regional patterns within and downwind of the ICE boxes, we also conduct time series analyses in two small ATM boxes. The boxes are chosen because the two reanalyses do not have the same grid size and the boxes of roughly 110 km times 110 km (see Tab. 1) ensure that the reanalysis datasets cover almost the same area. To be able to attribute the observed trends in atmospheric variables to sea ice changes we consider only times with wind from north-east (30 ° to 60 °) for WNB and from west to north (-45 ° to 15 °) for GRL, which is roughly perpendicular to the ice edge and thus represents off-ice flow conditions. In the following we use the expression off-ice only in this sense, for which the fetch over open water is largest. By comparing these results for off-ice flow to the results using data for all other wind directions we are able to separate effects related to sea ice cover from other effects influencing atmospheric conditions, e.g. warm-air intrusions from the south or changes in ocean currents. We place the ATM boxes in those regions where we observe the largest trend differences between off-ice flow and other wind directions (see Sect. 3.1 for details), which is close to the location of the sea ice edge during the maximum observed regional sea ice extent at the downwind side of the ICE boxes.

Tetzlaff et al. (2014) determined the distance an air parcel traveled over open ocean in the WNB region and showed that air temperatures downstream of this region correlate with this so-called fetch length. Here, we also calculate the WNB fetch length along the thick green line indicated in Fig. 1 and consider grid cells with less than 70 % sea ice concentration as open water.

Table 1. Coordinates of the Western Nansen Basin (WNB) and Greenland sea (GRL) boxes considered for the statistical analyses of sea ice (ICE) and atmospheric (ATM) conditions (see also Fig. 1).

Region	Latitude	Longitude
WNB		
ICE box	80.5 - 83.0 °N	15.0 - 65.0 °E
ERA5 ATM box	79.9 - 80.9 °N	5.9 - 13.1 °E
MERRA-2 ATM box	79.8 - 80.8 °N	5.9 - 12.8 °E
GRL		
ICE box	70.0 - 78.0 °N	21.5 - 0.0 °W
ERA5 ATM box	69.4 - 70.4 °N	18.1 - 14.9 °W
MERRA-2 ATM box	69.3 - 70.3 °N	17.8 - 14.7 °W

2.4 Statistical methods

We calculate the slopes b of all trend lines using a linear least-squares regression. The uncertainty of the slopes is given as the 95 %-confidence interval according to a t-test. Using the t-value t for $n-2$ degrees of freedom (with $n = 31$ years) and the standard error s_b of the slope, the confidence interval is calculated as $\pm s_b\, t_{n-2}$.

https://doi.org/10.5194/tc-2022-185
Preprint. Discussion started: 4 October 2022

Correlations are calculated to determine the relationship between sea ice and meteorological variables. Since the relationship is non-linear (see Fig. 9), we use the Spearman's rank correlation coefficient r, which is a measure of the strength of a monotonic relationship. A t-test is applied for significance testing of correlation coefficients. To test whether correlation coefficients differ significantly from each other, we use the formula suggested by Steiger (1980) for dependent correlation coefficients.

3 Results

In this section we analyze trends in atmospheric variables and sea ice concentrations in the Fram Strait region. Trends of atmospheric temperature, humidity and wind speed for both the WNB and GRL regions are presented in Sect. 3.1, followed by sea ice trends in Sect. 3.2 Finally, to assess the impact of the observed sea ice variability on atmospheric conditions, we calculate correlation maps (Sect. 3.3).

3.1 Trends in meteorological variables

To identify changes of atmospheric conditions in the Fram Strait regions, we calculate trends maps using data from both reanalyses averaged over January to March for each year from 1992 to 2012. Since the maps for both reanalyses look very similar, we only show the results based on ERA5. Generally, trends for wind speed are mostly not significant and thus, trend maps for wind are not presented. The result for wind trends in the ATM boxes are discussed later in this section.

Changes of atmospheric quantities could be related either to changing surface conditions, such as sea ice cover or sea surface temperature, or to dynamic changes of the atmosphere, for example during warm-air intrusions. We compare trends calculated using periods with off-ice flow, i.e. north-easterly (westerly to northerly) winds for WNB (GRL), to those with all other wind directions. If trends are larger for off-ice flow and local maxima can be found in the considered regions, this indicates that changing conditions in the upstream sea ice regions is the most probable reason for the observed atmospheric changes.

Off-ice flow conditions are present for about 16 % of the time in the WNB region (north-easterly winds) and for about 33 % in the GRL region (westerly to northerly winds), which is roughly double of what would be expected for a uniform distribution of wind directions. Trends of the frequencies of off-ice flow are only significant in a region north-west of Svalbard (Fig. 2). Here, trends weaken with distance from Svalbard from about -5 to -1 % per decade. A trend of about -3 % per decade results in roughly a halving of the off-ice flow frequency over the 31-year period in this area. Trends in the GRL region are not significant at the 95 %-level (not shown).

Fig. 3 shows temperature and humidity trends in the WNB region for both off-ice flow and other wind directions and their respective differences. For north-easterly flow, the largest temperature trends are observed north and north-east of Svalbard , so over the Whaler's bay polynya region, and exceed 4 K per decade. Along the off-ice flow direction towards south-west, trends gradually decrease but are still above 1 K per decade 300 km downstream. It is interesting to note that positive air temperature trends are not restricted to open ocean regions but also extend westwards over regions with closed sea ice cover. For specific humidity, the pattern of the trends for off-ice flow looks very similar to the temperature trends (Fig. 3b) with a maximum exceeding 25 $\mathrm{g\,kg^{-1}}$ per decade.

https://doi.org/10.5194/tc-2022-185
Preprint. Discussion started: 4 October 2022

The Cryosphere Discussions
Open Access
EGU

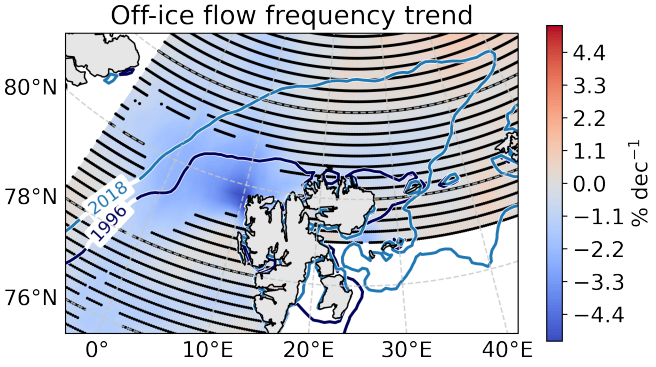

Figure 2. Trend maps in the greater WNB region for the frequency of off-ice flow (30°-60°) based on ERA5 wind directions for January to March of the years 1992 to 2022. Dotted areas are not significant at the 95 %-level. Blue lines denote the 80 % SSM/I-ASI sea ice concentration contours averaged from January to March for two years with large and small SIE, respectively.

Trends calculated using periods with all other wind directions show less distinct features with gradually decreasing trend values towards the south-west (Fig. 3c,d). Difference maps (Fig. 3e,f) indicate that trends for off-ice flow are more than 1 K and 0.1 $\mathrm{g\,kg^{-1}}$ per decade larger in a region north-west of Svalbard extending more than 300 km towards west and south. It is also notable that the largest trend differences for off-ice flow and other wind directions are not found in the region of the overall maximum trends, but rather in the region north-east of Svalbard. These are hints that temperature and humidity changes are indeed related to upstream sea ice changes rather than to local conditions.

While in the WNB region trends for off-ice flow are largest directly at the ice edge and decrease further downstream and thus southward, we find the largest trends for off-ice flow in the GRL region in areas that are covered by sea ice in only some of the years (Fig. 4a,b). The maximum trends of more than 1.5 K (0.15 $\mathrm{g\,kg^{-1}}$) per decade for temperature (humidity) are located along the 80 % sea ice contour from 1996, which was a year with large sea ice extent. The local maximum extends to the region south and south-east of Jan Mayen island, which is south of the area covered by the Odden ice tongue in some of the considered years. When comparing trends for off-ice flow to trends for all wind directions (Fig. 4e,f) we also see a pattern that is related to the Odden ice tongue, with larger trends for off-ice flow south of the Odden region. For humidity, trends in the Odden region are larger for all other wind directions which indicates that they are not related to local sea ice cover but probably to more frequent or stronger warm-air intrusions of humid air from the south.

In the following, we study time series of trends in more detail and facilitate the comparison of results for the two reanalyses by selecting smaller focus areas (ATM boxes). The boxes are chosen such that - despite different grid sizes - almost the same areas are included in both reanalyses. We place these ATM boxes in regions with the largest trend difference between conditions with off-ice flow and other wind directions. As a result, the ATM box for the WNB region is located at the north-western corner of Svalbard and for the GRL region close to the ice edge, south-west of the Odden ice tongue region. Corresponding time series of January to March means for each year averaged over the ATM boxes are presented in Figure 5 and trends with corresponding 95 % confidence intervals are listed in Tab. 2.

https://doi.org/10.5194/tc-2022-185
Preprint. Discussion started: 4 October 2022

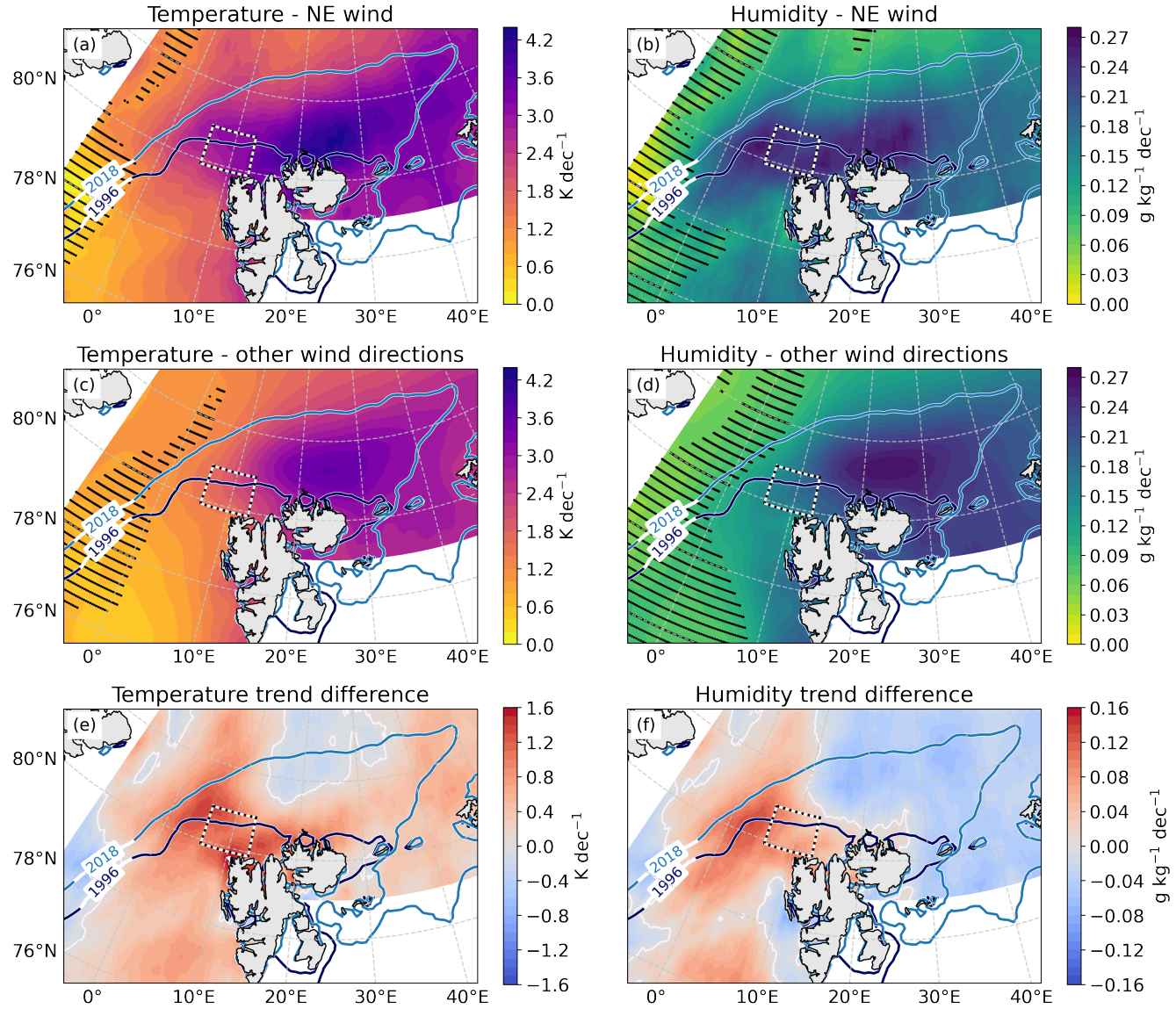

Figure 3. Trend maps in the greater WNB region for ERA5 air temperature (a,c) and specific humidity (b,d) for January to March of the years 1992 to 2022 using only periods with north-easterly winds (a,b) and using periods with all other wind directions (c,d). Dotted areas are not significant at the 95 %-level. Blue lines denote the 80 % SSM/I-ASI sea ice concentration contours averaged from January to March for two years with large and small SIE, respectively. Panel (e) shows the differences of air temperature trends using north-easterly winds and the trends using all other wind directions (panel (a) minus panel (c)) and panel (f) shows the corresponding trend differences for specific humidity. Black and white dashed boxes are ATM boxes used for time series analyses in Fig. 5 and Tab. 2.

https://doi.org/10.5194/tc-2022-185
Preprint. Discussion started: 4 October 2022

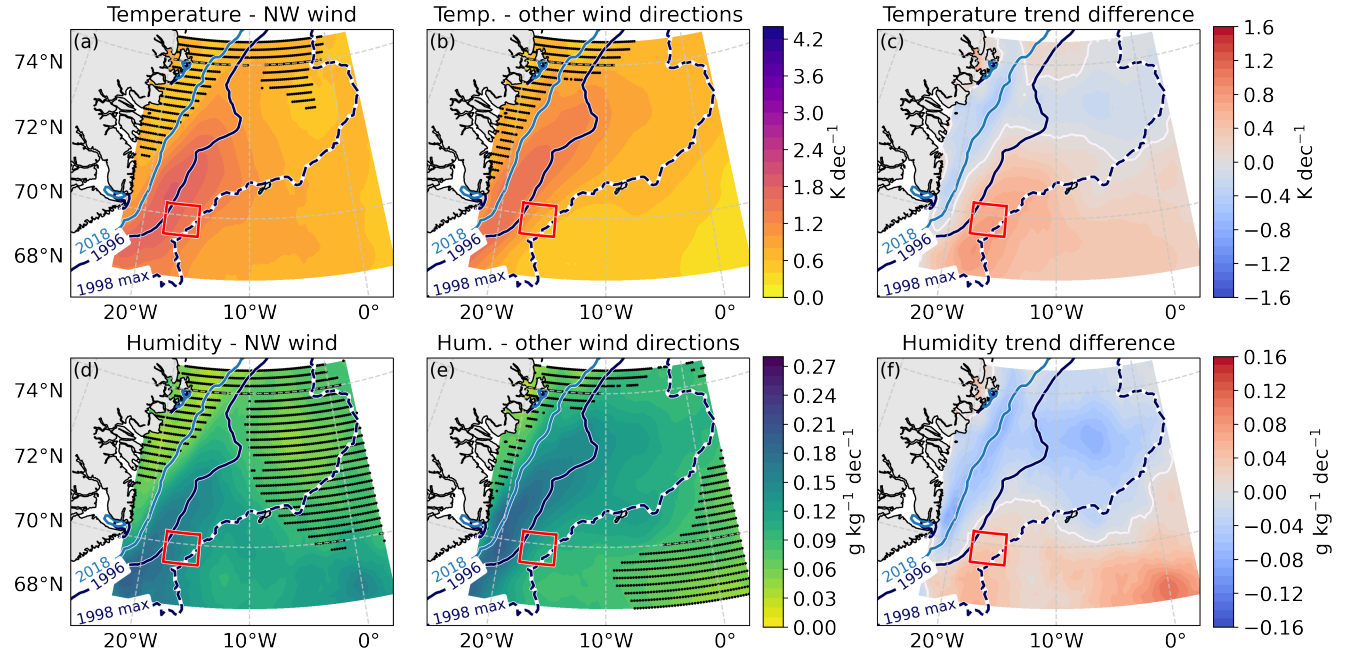

Figure 4. Trend maps in the GRL region for ERA5 air temperature (a,b) and specific humidity (d,e) for January to March of the years 1992 to 2022 using only periods with westerly to northerly winds (a,d) or periods with the remaining other wind directions (b,e). Dotted areas are not significant at the 95 %-level. Trend differences between the left and the middle columns (periods with westerly to northerly winds minus others) are shown in the right column (c,f). Blue lines denote the 80 % SSM/I-ASI sea ice concentration contours averaged from January to March for two years with large and small SIE, respectively. The dashed contour shows the maximum SIE between January and March in 1998, which roughly represents a typical outline of the Odden ice tongue. Red boxes are ATM boxes used for time series analyses in Fig. 5 and Tab. 2.

In the WNB ATM box, air temperatures and specific humidity show significant positive trends with slightly smaller numbers for MERRA-2 than for ERA5 (Fig. 5) for off-ice flow. Overall, the air temperature increased by 9.2 K (7.1 K) during the 31 years and the specific humidity by 0.73 g kg^{-1} (0.58 g kg^{-1}) for ERA5 (MERRA-2). The wind speed change is close to zero and not significant at the 95 %-level for both reanalyses. Considering all other wind directions, trends for temperature are about 37 % smaller for ERA5 and 28 % smaller for MERRA-2. For humidity, trends for all other wind directions are 28 % (19 %) smaller for ERA5 (MERRA-2) than for off-ice flow.

Temperature and humidity trends in the GRL ATM box are generally smaller than for WNB but still significant at the 95 %-level (Tab. 2). Both reanalyses agree well on the magnitude of the trends for off-ice flow with overall temperature and humidity increases of up to almost 5 K and 0.5 g kg^{-1} within 31 years, respectively. Wind speed trends are negative but only barely significant with an overall decrease of up to 2.0 m s^{-1} within 31 years. As for WNB, trends calculated using periods with all other wind directions are more than 40 % (20 %) smaller for temperature (humidity) than for off-ice flow.

https://doi.org/10.5194/tc-2022-185
Preprint. Discussion started: 4 October 2022

The Cryosphere Discussions
Open Access
EGU

Table 2. Trends of meteorological variables in the WNB and GRL regions based on ERA5 and MERRA-2 reanalysis data. Trends are calculated either using only periods with flow from north-east for WNB and from west to north for GRL ("off-ice") or using only periods with all other wind directions, which are not off-ice ("other"). Confidence intervals are calculated based on a t-test with 95 % confidence level.

Meteorological variable	ERA5 off-ice	ERA5 other	MERRA-2 off-ice	MERRA-2 other
WNB				
Temperature trend (K dec^{-1})	3.0 ± 1.3	1.9 ± 1.3	2.3 ± 1.4	1.6 ± 1.2
Specific humidity trend (g kg^{-1} dec^{-1})	0.24 ± 0.11	0.17 ± 0.12	0.19 ± 0.13	0.15 ± 0.12
Wind speed trend (m s^{-1} dec^{-1})	0.0 ± 0.3	0.0 ± 0.2	-0.4 ± 0.4	-0.2 ± 0.2
GRL				
Temperature trend (K dec^{-1})	1.6 ± 0.7	0.9 ± 0.5	1.5 ± 0.6	0.7 ± 0.4
Specific humidity trend (g kg^{-1} dec^{-1})	0.15 ± 0.08	0.12 ± 0.08	0.15 ± 0.07	0.11 ± 0.07
Wind speed trend (m s^{-1} dec^{-1})	-0.5 ± 0.3	-0.1 ± 0.3	-0.7 ± 0.3	-0.3 ± 0.3

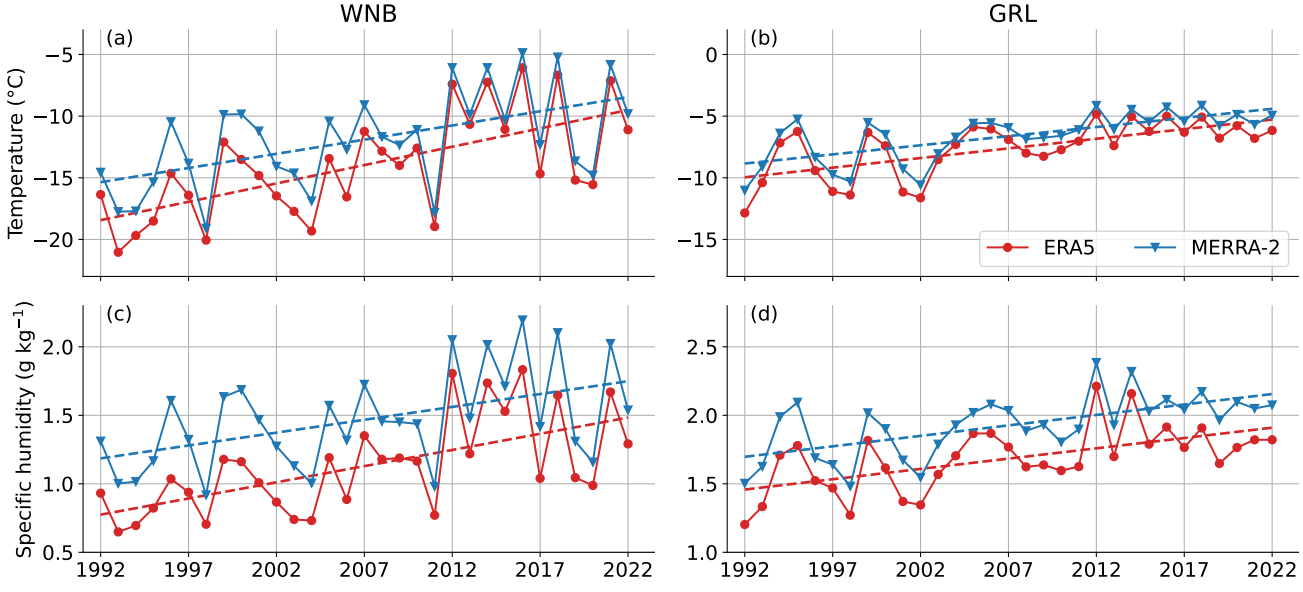

Figure 5. January to March averages of air temperature (a,b) and specific humidity (c,d) based on ERA5 (red) and MERRA-2 (blue) reanalyses for off-ice flow - i.e. north-easterly flow in the WNB region (a,c) and westerly to northerly flow in the GRL region (b,d). Dashed lines indicate trends.

Our comparison of trends calculated based on ERA5 and MERRA-2 data indicate that the results are robust with respect to the choice of reanalysis dataset. Especially in the GRL region, trend values are almost identical. The largest trend differences

https://doi.org/10.5194/tc-2022-185
Preprint. Discussion started: 4 October 2022

occur for temperature in the WNB ATM box. It is evident from Fig. 5a that MERRA-2 temperatures are up to 3 K higher than ERA5 temperatures in the first half of the considered period, while differences decrease to about 1 to 1.5 K in the second half. Thus, even though trends are smaller for MERRA-2, overall temperatures in the last decade were even larger than for ERA5.

3.2 Sea ice trends

Trends of sea ice concentration based on SSM/I-ASI data indicate that in the 31 years since 1992 sea ice cover has declined in large parts of the Fram Strait region (Fig. 6). The largest trends exceeding -20 % per decade are observed in the Barents sea south-east of Svalbard, in the region of the Whaler's Bay polynya north of Svalbard and in the region of the Odden ice tongue in the Greenland sea. The latter two regions coincide with the regions analyzed in Sect. 3.1, where we identified regions of the largest observed temperature and humidity trends at the north-west corner of Svalbard and south-west of the Odden region. We now focus on those regions located upstream of these ATM boxes for off-ice flow conditions to identify possible similarities between sea ice and atmospheric trends

We calculate average ice concentrations within the ICE boxes in Fig. 1 and 6 for the months January to March. Both the WNB and the GRL regions exhibit decreasing trends since 1992 (Fig. 7). In the WNB region the trend is -10.0 $\pm$ 3.5 % per decade with changing variability over time. In the 1990s, inter-annual variability was small with almost constant average sea ice concentrations around 90 %. Between 2000 and 2011 the variability increased and values approached 80 %. After 2012, we observe another shift in mean sea ice conditions with a strong inter-annual variability and values ranging from less than 60 % to about 85 %.

Tetzlaff et al. (2014) calculated the polynya or fetch length as a measure for daily sea ice conditions in the WNB region until the year 2014. Here, we extent their time series until the year 2022 (Fig. 8). While WNB fetch lengths exceeding 600 km did not occur in the 1990s and 2000s, such high values were much more common from 2012 onward. However, WNB fetch lengths during the last 10 years were highly variable with a more closed-up polynya in 2015 and 2020, for example. This explains the higher variability of mean sea ice concentrations in Fig. 7. When looking at WNB fetch length, 2022 was an exceptional year, even though average sea ice concentrations were not among the 5 lowest observed years. WNB fetch values exceeded 830 km during four days in January and two days in March 2022. The only other period with such high values was during the first days of January of 2013, however, the sea ice cover quickly closed up during the next weeks in this year.

In the GRL region the trend is also negative with -4.3 $\pm$ 3.1 % per decade (Fig. 7). It is smaller than in the WNB region, which is partly because the GRL ICE box contains open ocean areas and thus the maximum observed average sea ice concentration is more than 10 % lower than for the WNB region. The inter-annual variability is generally larger in the GRL region and contrary to the WNB region the largest variability is observed before 2002. This can be explained by the presence of the Odden ice tongue, which increases the average ice concentration in this region. From Fig. A1 it is evident that for example 1997 and 1998 were years with a large Odden ice tongue and also two of the years with the overall largest observed mean sea ice concentrations since 1992. After 2006 the Odden ice tongue does not occur frequently any more and thus the inter-annual sea ice variability decreases.

https://doi.org/10.5194/tc-2022-185
Preprint. Discussion started: 4 October 2022

The Cryosphere
Discussions
Open Access
EGU

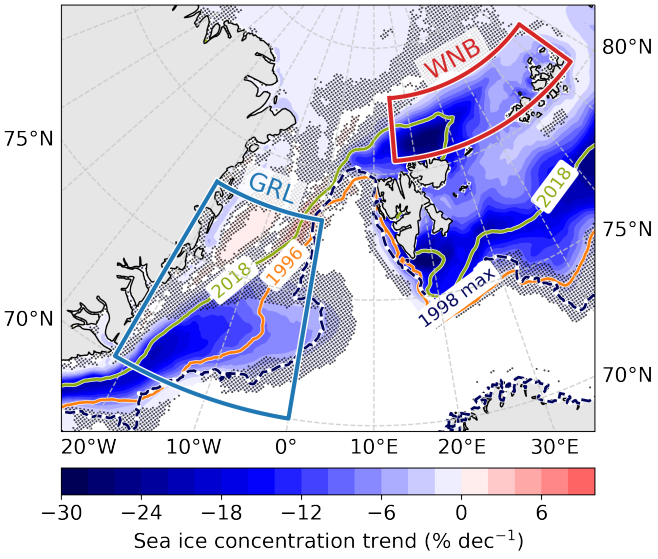

Figure 6. Sea ice concentration trends based on SSM/I-ASI data for the years 1992 to 2022. Dotted areas are not significant at the 95 %-level. Colored lines denote the 80 % SSM/I-ASI sea ice concentration contours averaged from January to March for two years with large and small SIE, respectively. The dashed contour shows the maximum SIE between January and March in 1998, which roughly represents a typical outline of the Odden ice tongue. ICE boxes used for the calculation of sea ice concentration time series are shown in blue for the GRL region and in red for the WNB region.

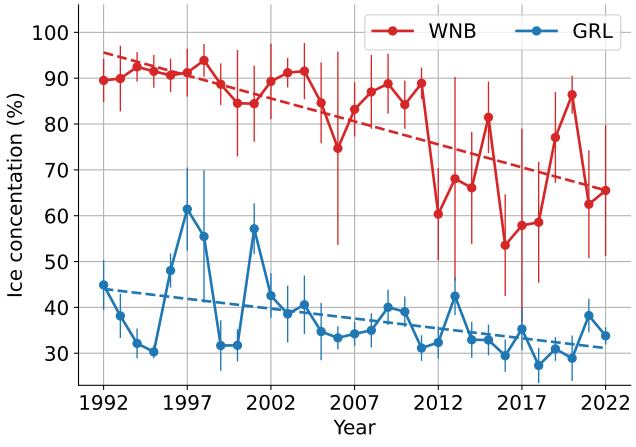

Figure 7. Winter mean sea ice concentrations from SSM/I-ASI in the ICE boxes in Fig. 1 and 6 for the WNB and GRL regions averaged from January to March. Errorbars denote standard deviations of daily values. Dashed lines represent linear trends.

https://doi.org/10.5194/tc-2022-185
Preprint. Discussion started: 4 October 2022

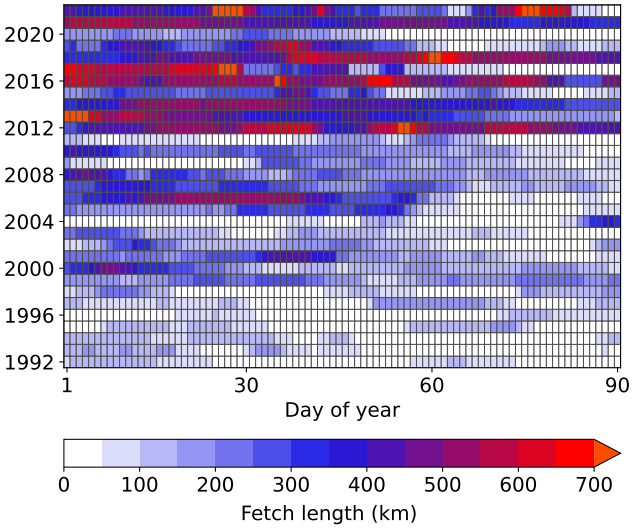

Figure 8. Daily fetch length over the WNB polynya region. Updated from Tetzlaff et al. (2014).

3.3 Assessing relationships between sea ice trends and meteorological variables

In the previous two sections we demonstrated that winter sea ice concentrations and atmospheric temperatures and humidity show significant trends since 1992 in the WNB and GRL regions. For off-ice flow in both regions, Spearman rank correlations of about r =-0.8 indicate a strong relationship between temperatures and sea ice cover and a slightly weaker one for humidity. In this section, we analyze the spatial extent of these correlations in more detail.

For this purpose, we follow the method of Tetzlaff et al. (2014) who analyzed ERA-Interim near-surface temperatures averaged over the winter season from January to March for the years 1992 to 2014 at three grid points in the region north-west of Svalbard and found high correlations with the open-water fetch over the WNB region. In Fig. 9a we extend their analysis to the year 2022 and use a higher temporal resolution with January to March monthly means instead of winter means. We find similarly high Spearman rank correlations of r =0.86 also for the extended period at a point north-west of Svalbard (see triangles in Fig. 10), which decreases to r =0.58 at a point more than 200 km downstream. We performed a similar analysis to determine the relationship between average WNB sea ice concentration and atmospheric temperatures and found very similar correlations at the two considered points (Fig. 9b). Thus, instead of using the open-water fetch as in Tetzlaff et al. (2014), we consider sea ice concentrations in the ICE boxes for the following correlation analysis.

As a next step, we then extend our correlation analysis to larger areas in the WNB and GRL regions. This allows us to identify regions where the impact of upstream sea ice concentration is largest. The squared correlation coefficient r^2 can also be used as a measure of the observed variance of the meteorological variables that can be explained by sea ice variability. As

https://doi.org/10.5194/tc-2022-185
Preprint. Discussion started: 4 October 2022

The Cryosphere Discussions
Open Access
EGU

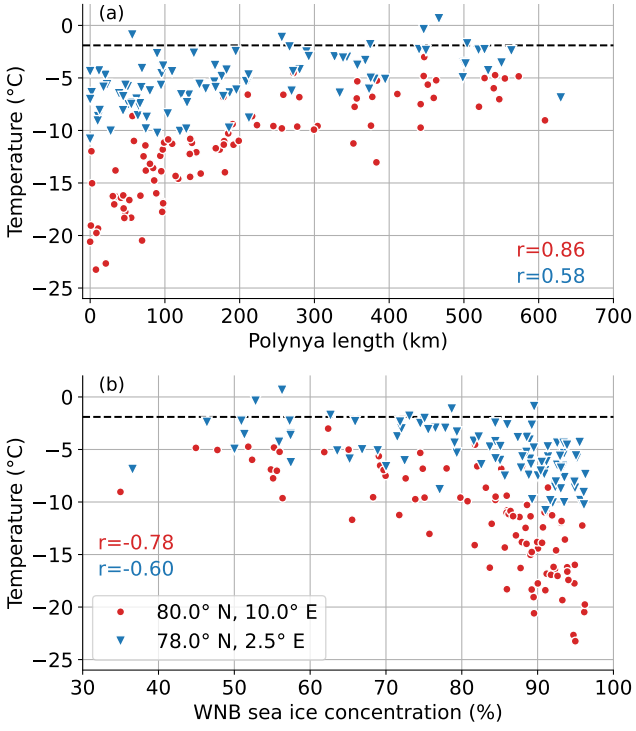

Figure 9. ERA5 air temperature at two locations (marked with triangles in Fig. 10) averaged monthly for periods with north-easterly flow as function of WNB fetch (a) and average WNB sea ice concentration (b). Numbers are Spearman rank correlations.

for the trends in Sect. 3.1, the maps based on ERA5 and MERRA-2 look very similar and thus we only present the ERA5 results, here.

Correlation maps for WNB for off-ice flow are presented in Fig. 10. As for the atmospheric trends (Sect. 3.1), the general patterns look very similar for temperature and humidity with the strongest negative correlation exceeding -0.85 for temperature and -0.8 for humidity in the area north-east of Svalbard over the center of the Whaler's Bay polyna. The region with the largest significant differences between off-ice flow and other wind direction is located at the north-west corner of Svalbard, which is directly downstream of the sea ice edge in years with a large SIE (not shown). Off-ice flow consists of relatively cold and dry air masses becoming warmer and more humid the longer they are in contact with open ocean. A smaller sea ice concentration means more open water areas and thus correlations between sea ice cover and air temperature and humidity are negative. Maximum negative Spearman rank correlations in this area exceed -0.8 for temperature and -0.75 for humidity. This means that about two thirds of the observed variance can be explained by WNB sea ice variability, which is about 10 % larger than for other wind directions. Correlations decrease with a similar rate with downstream distance for both temperature and humidity until correlations are not significant any more at about 500 km downstream. We also observe smaller correlations directly at the

https://doi.org/10.5194/tc-2022-185
Preprint. Discussion started: 4 October 2022

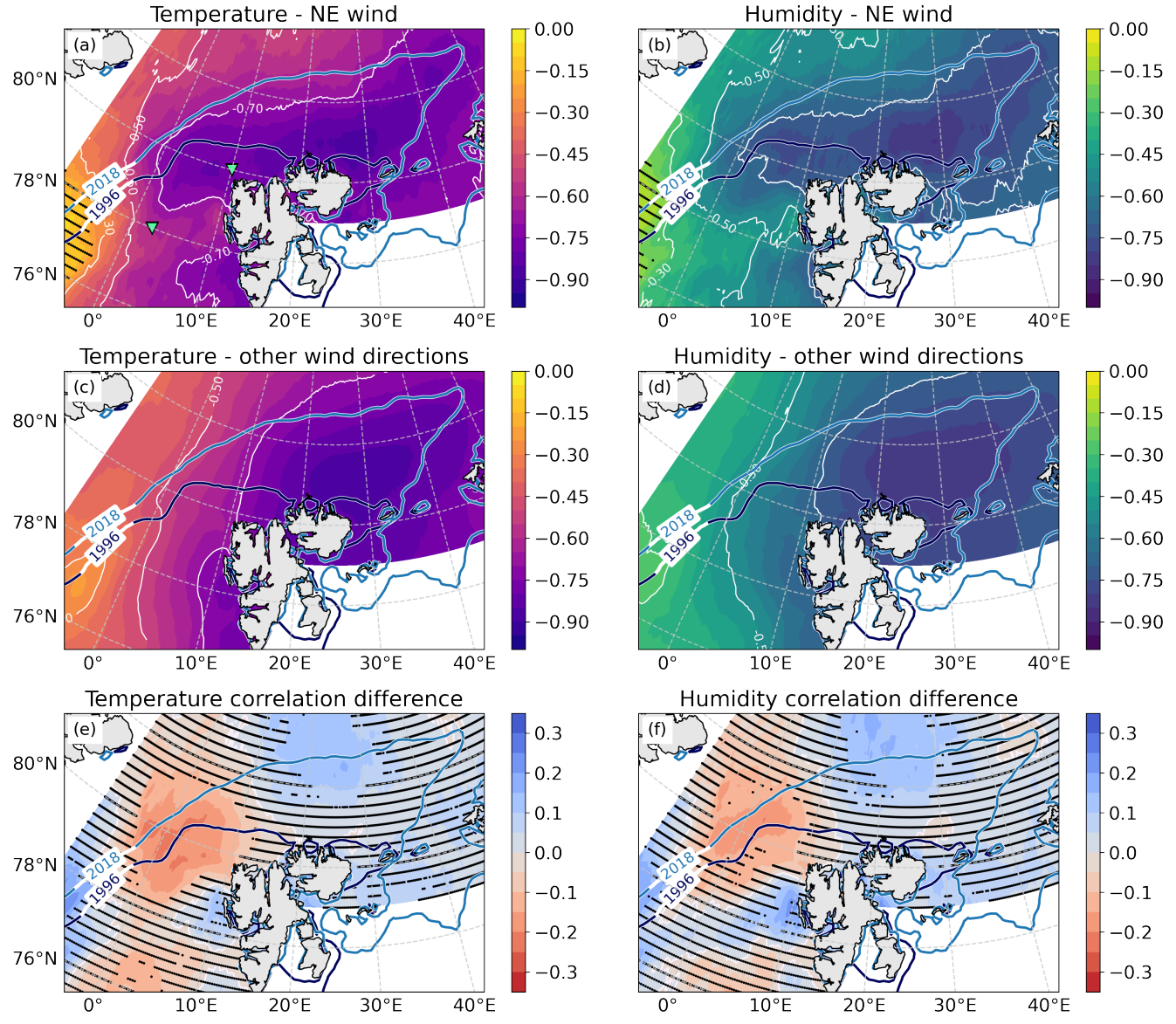

Figure 10. Spearman rank correlation coefficients between monthly WNB sea ice concentrations and air temperatures (a,c) and specific humidity (b,d) from ERA5 averaged for periods with north-easterly wind directions (a,d) and all other wind directions (b,e). Panels (c) and (f) show correlation differences between off-ice flow and other wind directions. Dotted areas are not significant at the 95 %-level. Blue lines denote the 80 % SSM/I-ASI sea ice concentration contours averaged from January to March for two years with large and small SIE, respectively. Triangles indicate the locations used in Fig. 9.

west coast of Svalbard, which can be attributed to a sheltering effect of the Svalbard land mass. Over land, air masses flowing from north-east do not experience any further warming an moistening and thus correlations decrease.

https://doi.org/10.5194/tc-2022-185
Preprint. Discussion started: 4 October 2022

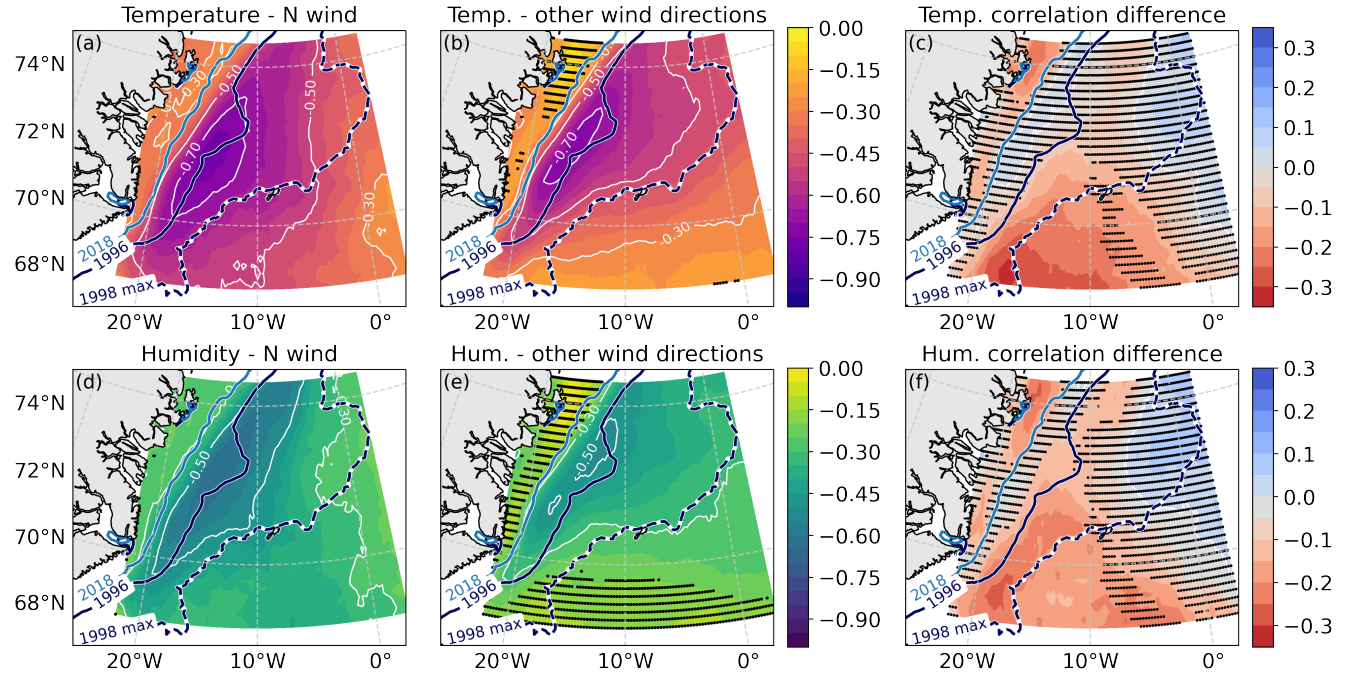

Figure 11. Spearman rank correlation coefficients between monthly GRL sea ice concentrations and air temperatures (a-c) and specific humidity (d-e) from ERA5 averaged for periods with westerly to northerly wind directions (a,d) and all other wind directions (b,e). Panels (c) and (f) show correlation differences between off-ice flow and other wind directions. Dotted areas are not significant at the 95 %-level. Blue lines denote the 80 % SSM/I-ASI sea ice concentration contours averaged from January to March for two years with large and small SIE, respectively. The dashed contour shows the maximum SIE between January and March in 1998, which roughly represents a typical outline of the Odden ice tongue.

The corresponding correlation maps for the GRL region are presented in Fig. 11. As for the WNB region, the observed patterns look similar to the trends of meteorological variables presented in Sect. 3.1. Negative correlations are largest in the region that is only covered by sea ice in some of the considered years with a maximum exceeding -0.7 for temperature and -0.6 for humidity. This means that up to half of the observed variance can be explained by sea ice variability for off-ice flow. Correlation differences are most pronounced and only significant south-west of the Odden region where the explained variance is more than 10 % larger for periods with off-ice flow than for all other wind directions (Fig. 11e,f).

4 Discussion and conclusions

We studied recent regional trends in near-surface atmospheric variables in the Northern Fram Strait region in winter and their connection to regional sea ice cover. To disentangle the impact of sea ice changes from other factors influencing atmospheric conditions we analyzed data for off-ice flow and other wind directions separately and compared the results.

https://doi.org/10.5194/tc-2022-185
Preprint. Discussion started: 4 October 2022

As a first step we calculated trends of atmospheric temperature, specific humidity and wind speed at about 10 m height based on ERA5 and MERRA-2 reanalysis data in two sub-regions: the first one north-east of Svalbard in the Western Nansen Basin (WNB) and the second one in the Greenland sea (GRL). Trends for temperature and specific humidity are positive and significant in regions, while wind speed trends are slightly negative but mostly not significant. Generally, ERA5 and MERRA-2 agree well on the magnitude and the pattern of the trends. For both temperature and humidity, we find the largest trends in the WNB region north-east of Svalbard over the center of the Whaler's Bay polynya, which gradually decrease towards the south-west. The largest differences for off-ice flow and other wind directions can be found at the north-western corner of Svalbard - even extending westward over sea-ice covered regions. In that area, 31-year trends amount to 3.0 $\mathrm{K\,dec^{-1}}$ for temperature and 0.24 $\mathrm{g\,kg^{-1}\,dec^{-1}}$ for humidity for off-ice flow. These values exceed the observed trends for all other wind directions by about one third, indicating that a significant part of the observed atmospheric changes is related to conditions over the upstream sea ice region. In the GRL region we find the largest trends for off-ice flow close to the ice edge in areas that are covered by sea ice in only some of the years, specifically south and south-west of the Odden ice tongue region. In these areas, temperature and humidity trends amount to 1.6 K and 0.16 $\mathrm{g\,kg^{-1}}$ per decade for off-ice flow, respectively. As for WNB, this is almost one third larger than trends calculated using periods with all other wind directions.

Temperature trends for similar regions have also previously been calculated by other authors. Johannessen et al. (2016) analyzed the Nansen surface air temperature dataset, which incorporates data from land stations, buoys and ship measurements in a larger region containing the Greenland and Barents seas and the Fram Strait region. They found that running 30-year temperature trends increased since the 1970s with a value exceeding 1.5 K per decade between 1985 to 2014. Even though they considered a larger region, our results for WNB indicate that temperature trends might have further increased since 2014. Based on air temperature data from the NCEP-DOE reanalysis from 1979 to 2016, Wang et al. (2019) reported trends of about 1.5 K per decade in the GRL region and of about 2 K at the north-west corner of Svalbard, which is in line with our findings.

As a second step, we calculated mean January to March sea ice conditions based on SSM/I-ASI sea ice concentration data from 1992 to 2022 averaged over two boxes for the two considered regions. WNB shows a strong declining trend of -10.0 % per decade with increasing inter-annual variability within the last 10 years. While the ice edge was mostly located at the north-west corner of Svalbard during the 1990s, it retreated by more than 500 km toward the north-east during many days in January to March since 2012. 2022 was an extreme year since the open water fetch exceeded 800 km during two separate weeks. The event in March was a consequence of a period with strong southerly winds causing a warm-air intrusion into the Arctic across the Fram Strait region.

The negative sea ice trend in the GRL region is also significant but with -4.7 % per decade smaller than for WNB, which is partly due to a larger fraction of open ocean within the GRL box already at the beginning of the analysed period. Inter-annual variability is largest within the first half of the considered period, which is related to the presence of the Odden ice tongue in some of the years before 2006. Our results are in line with sea ice trends in the winter seasons reported by previous studies. Based on NASA-Team passive microwave sea ice concentration data from 1979 to 2018, Stroeve and Notz (2018) found trends of the same order of magnitude in both the WNB and GRL regions for March. Wang et al. (2019) considered a slightly larger

https://doi.org/10.5194/tc-2022-185
Preprint. Discussion started: 4 October 2022

region in the Greenland sea, which extended further south and thus contained more open ocean areas. Consequently, they found a slightly smaller trend of about -2 % per decade in winter from 1982 to 2016.

Additionally, we conducted a spatial analysis of trends in meteorological variables and their correlations to the upstream ice conditions. The results indicate that the impact of changing sea ice conditions on air temperature and humidity is largest at the ice margins but besides that it is not localized and extends hundreds of kilometers further downstream. Generally, correlation maps display great similarities with trend maps. In the WNB region, we also find the largest differences between off-ice flow and other wind directions at the north-western corner of Svalbard. In this area, correlations for off-ice flow exceed -0.8 for both temperature and humidity and thus sea ice changes in the upstream region can explain up to two thirds of the observed variability in this region, which is about 10 % larger than for other wind directions.

In the GRL region, the largest trends and correlations are found in the region containing sea ice in only some of the years. Up to 50 % of observed temperature and humidity variability can be explained by local sea ice changes for off-ice flow, which is about 10 % larger than for other wind directions. A secondary local maximum can also be found in the region south of the Odden ice tongue. Another study by Wang et al. (2019) also correlated atmospheric temperatures with sea ice conditions in all seasons and found a value of -0.46 for the whole Greenland sea region, which is slightly smaller than our maximum values of about r =-0.7. Since they averaged over a much larger region and did not consider different wind directions separately, they were not able to study more local effects and specifically the impact of upstream sea ice conditions during off-ice flow.

Our analyzes show that the impact of a decreasing sea ice cover in the Fram Strait region is largest in the marginal sea ice zone for off-ice flow during cold air outbreaks. By comparing our results for off-ice flow to those using all wind directions, we were able to identify regions for which increasing temperatures and humidity can be clearly attributed to uptream sea ice conditions. The occurrence of maximum trends at the sea ice margin, where sea ice changes a lot, is a clear hint to the important role of declining sea ice cover for the observed atmospheric trends.

A plausible explanation for the observed atmospheric changes is the increased atmospheric convection and related boundary-layer warming when the cold and dry air originating from the Central Arctic flows over extended areas of open ocean. Such events have been documented, e.g. for the Whaler's Bay polynya region by Tetzlaff et al. (2014). Even though our results suggest the important role of sea ice conditions for atmospheric warming and moistening, with our present analysis we cannot exclude further possible explanations for the observed atmospheric trends. For example, cases when warm air is advected first to the north and flowing back to the south afterwards might impact on our correleations. Also, changing ocean currents might increase sea surface temperatures in regions of a retreating sea ice margin. The investigation of such impact factors can be the topic of future extended work. Our analyses revealed an ongoing decrease of sea ice extent in the wider Fram Strait region and a concurrent increase of near-surface atmospheric temperature and humidity in winter. Studying related changes to the structure of the atmospheric boundary layer and to cloud processes in this region is an emerging topic, which will be partly addressed using data from the HALO-(AC)^3 campaign (Wendisch et al., 2021) that took place in spring 2022 in this region.

https://doi.org/10.5194/tc-2022-185
Preprint. Discussion started: 4 October 2022

The Cryosphere Discussions
Open Access
EGU

Appendix A: Odden ice tongue

The Odden ice tongue is a local phenomenon in the Greenland sea region where sea ice episodically covers a large area north of Jan Mayen island. It occurred most frequently before 1990 (Wadhams and Wilkinson, 1999; Comiso et al., 2001) but could still be observed in some of the years in our study period from 1992 to 2022. Figure A1 shows the standard deviation of daily sea ice concentration data from SSM/I-ASI from January to March, which allows for a good visual detection of the extent of the Odden ice tongue.

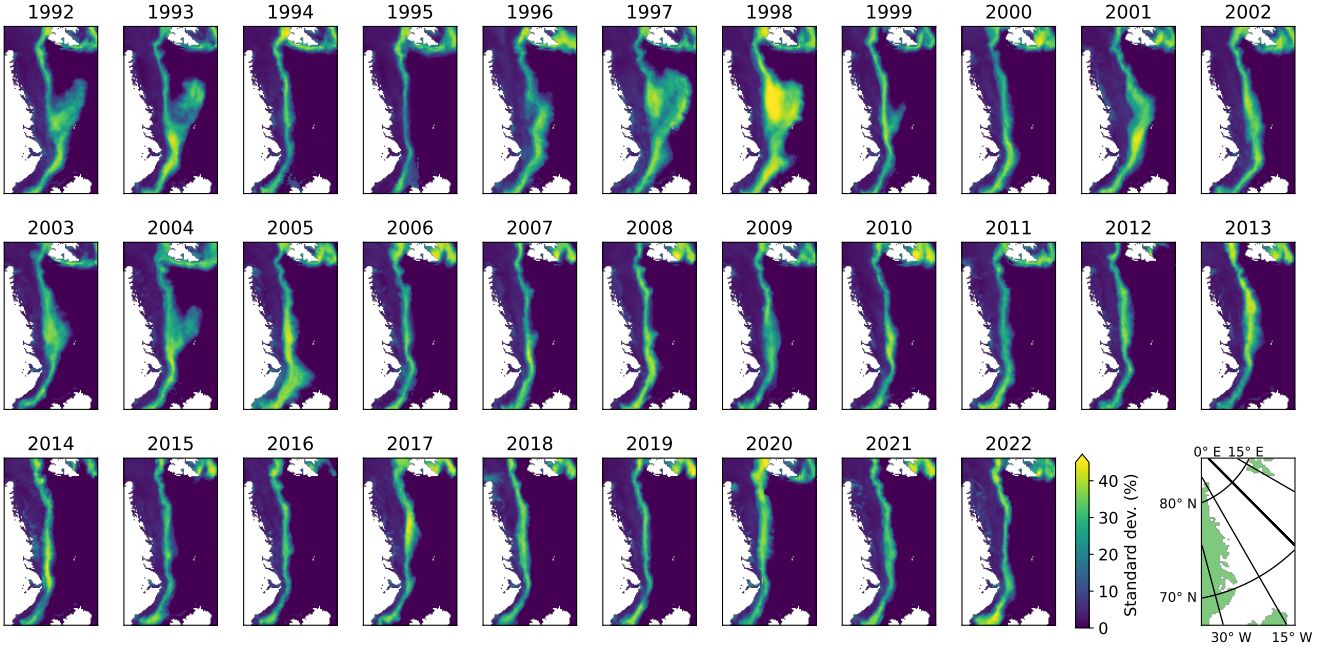

Figure A1. Standard deviation of daily SSM/I-ASI sea ice concentrations from January to March of each year in the Greenland sea and Fram Strait regions.

Code and data availability. Kaleschke, L., F. Girard-Ardhuin, G. Spreen, A. Beitsch, and S. Kern, ASI Algorithm SSMI-SSMIS sea ice concentration data, originally computed at and provided by IFREMER, Brest, France, were obtained as 5-day median-filtered and gap-filled product for 1992–2021 from the Integrated Climate Data Center (ICDC, icdc.cen.uni-hamburg.de, University of Hamburg, Hamburg, Germany). MERRA-2 data were provided by the Goddard Earth Sciences Data and Information Services Center (https://disc.gsfc.nasa.gov/). ERA5 profile data on model levels were obtained from ECMWF's MARS tape archive. The analysis scripts are available from the authors on request.

https://doi.org/10.5194/tc-2022-185
Preprint. Discussion started: 4 October 2022

Author contributions. AS and CL developed the original idea. AS analyzed and plotted the data. AS and CL interpreted the results and wrote the manuscript.

Competing interests. We declare that no competing interests are present.

Acknowledgements. This work was partly funded by the Deutsche Forschungsgemeinschaft (DFG, German Research Foundation) under Germany's Excellence Strategy – EXC 2037 'CLICCS - Climate, Climatic Change, and Society' – Project Number: 390683824, contribution to the Center for Earth System Research and Sustainability (CEN) of Universität Hamburg. It was also funded by the Deutsche Forschungsgemeinschaft (DFG; German Research Foundation) Project 268020496 TRR 172, within the Transregional Collaborative Research Center Arctic Amplification ((AC)^3). The results contain modified Copernicus Climate Change Service information (2014-2018). Neither the European Commission nor ECMWF is responsible for any use that may be made of the Copernicus information or data it contains.

https://doi.org/10.5194/tc-2022-185
Preprint. Discussion started: 4 October 2022

References

Chechin, D. G., Makhotina, I. A., Lüpkes, C., and Makshtas, A. P.: Effect of wind speed and leads on clear-sky cooling over Arctic sea ice during polar night, Journal of the Atmospheric Sciences, 76, 2481–2503, 2019.

Cohen, J., Screen, J. A., Furtado, J. C., Barlow, M., Whittleston, D., Coumou, D., Francis, J., Dethloff, K., Entekhabi, D., Overland, J., et al.: Recent Arctic amplification and extreme mid-latitude weather, Nature geoscience, 7, 627–637, 2014.

Comiso, J. C., Wadhams, P., Pedersen, L. T., and Gersten, R. A.: Seasonal and interannual variability of the Odden ice tongue and a study of environmental effects, Journal of Geophysical Research: Oceans, 106, 9093–9116, https://doi.org/10.1029/2000JC000204, 2001.

Dahlke, S., Hughes, N. E., Wagner, P. M., Gerland, S., Wawrzyniak, T., Ivanov, B., and Maturilli, M.: The observed recent surface air temperature development across Svalbard and concurring footprints in local sea ice cover, International Journal of Climatology, 40, 5246–5265, https://doi.org/https://doi.org/10.1002/joc.6517, 2020.

Gelaro, R., McCarty, W., Suárez, M. J., Todling, R., Molod, A., Takacs, L., Randles, C. A., Darmenov, A., Bosilovich, M. G., Reichle, R., Wargan, K., Coy, L., Cullather, R., Draper, C., Akella, S., Buchard, V., Conaty, A., da Silva, A. M., Gu, W., Kim, G.-K., Koster, R., Lucchesi, R., Merkova, D., Nielsen, J. E., Partyka, G., Pawson, S., Putman, W., Rienecker, M., Schubert, S. D., Sienkiewicz, M., and Zhao, B.: The Modern-Era Retrospective Analysis for Research and Applications, Version 2 (MERRA-2), Journal of Climate, 30, 5419 – 5454, https://doi.org/10.1175/JCLI-D-16-0758.1, 2017.

Global Modeling and Assimilation Office (GMAO): MERRA-2, Greenbelt, MD, USA, Goddard Earth Sciences Data and Information Services Center (GES DISC), https://doi.org/10.5067/VJAFPLI1CSIV, tavg1_2d_slv_Nx: 2d,1-Hourly,Time-Averaged,Single-Level,Assimilation,Single-Level–Diagnostics V5.12.4, Accessed: 28/04/2021, 2015.

Graversen, R. G., Mauritsen, T., Tjernström, M., Källén, E., and Svensson, G.: Vertical structure of recent Arctic warming, Nature, 451, 53–56, 2008.

Hersbach, H., Bell, B., Berrisford, P., Hirahara, S., Horányi, A., Muñoz-Sabater, J., Nicolas, J., Peubey, C., Radu, R., Schepers, D., Simmons, A., Soci, C., Abdalla, S., Abellan, X., Balsamo, G., Bechtold, P., Biavati, G., Bidlot, J., Bonavita, M., De Chiara, G., Dahlgren, P., Dee, D., Diamantakis, M., Dragani, R., Flemming, J., Forbes, R., Fuentes, M., Geer, A., Haimberger, L., Healy, S., Hogan, R., Hólm, E., Janisková, M., Keeley, S., Laloyaux, P., Lopez, P., Lupu, C., Radnoti, G., de Rosnay, P., Rozum, I., Vamborg, F., Villaume, S., and Thépaut, J.-N.: Complete ERA5: Fifth generation of ECMWF atmospheric reanalyses of the global climate, Copernicus Climate Change Service (C3S) Data Store (CDS). (Accessed on 13-04-2021), 2017.

Hersbach, H., Bell, B., Berrisford, P., Hirahara, S., Horányi, A., Muñoz-Sabater, J., Nicolas, J., Peubey, C., Radu, R., Schepers, D., Simmons, A., Soci, C., Abdalla, S., Abellan, X., Balsamo, G., Bechtold, P., Biavati, G., Bidlot, J., Bonavita, M., De Chiara, G., Dahlgren, P., Dee, D., Diamantakis, M., Dragani, R., Flemming, J., Forbes, R., Fuentes, M., Geer, A., Haimberger, L., Healy, S., Hogan, R. J., Hólm, E., Janisková, M., Keeley, S., Laloyaux, P., Lopez, P., Lupu, C., Radnoti, G., de Rosnay, P., Rozum, I., Vamborg, F., Villaume, S., and Thépaut, J.-N.: The ERA5 global reanalysis, Quarterly Journal of the Royal Meteorological Society, 146, 1999–2049, https://doi.org/10.1002/qj.3803, 2020.

Isaksen, K., Nordli, Ø., Førland, E. J., Łupikasza, E., Eastwood, S., and Niedźwiedź, T.: Recent warming on Spitsbergen—Influence of atmospheric circulation and sea ice cover, Journal of Geophysical Research: Atmospheres, 121, 11,913–11,931, https://doi.org/https://doi.org/10.1002/2016JD025606, 2016.

Ivanov, V. V., Alexeev, V. A., Repina, I., Koldunov, N. V., and Smirnov, A.: Tracing Atlantic Water signature in the Arctic sea ice cover east of Svalbard, Advances in Meteorology, 2012, https://doi.org/10.1155/2012/201818, 2012.

Johannessen, O. M., Kuzmina, S. I., Bobylev, L. P., and Miles, M. W.: Surface air temperature variability and trends in the Arctic: new amplification assessment and regionalisation, Tellus A: Dynamic Meteorology and Oceanography, 68, 28 234, https://doi.org/10.3402/tellusa.v68.28234, 2016.

Kaleschke, L., Lüpkes, C., Vihma, T., Haarpaintner, J., Bochert, A., Hartmann, J., and Heygster, G.: SSM/I Sea Ice Remote Sensing for Mesoscale Ocean-Atmosphere Interaction Analysis, Canadian Journal of Remote Sensing, 27, 526–537, https://doi.org/10.1080/07038992.2001.10854892, 2001.

Kern, S., Kaleschke, L., and Spreen, G.: Climatology of the Nordic (Irminger, Greenland, Barents, Kara and White/Pechora) Seas ice cover based on 85 GHz satellite microwave radiometry: 1992–2008, Tellus A: Dynamic Meteorology and Oceanography, 62, 411–434, https://doi.org/10.1111/j.1600-0870.2009.00457.x, 2010.

Lundesgaard, Ø., Sundfjord, A., and Renner, A. H. H.: Drivers of Interannual Sea Ice Concentration Variability in the Atlantic Water Inflow Region North of Svalbard, Journal of Geophysical Research: Oceans, 126, e2020JC016 522, https://doi.org/https://doi.org/10.1029/2020JC016522, e2020JC016522 2020JC016522, 2021.

Lüpkes, C., Vihma, T., Birnbaum, G., and Wacker, U.: Influence of leads in sea ice on the temperature of the atmospheric boundary layer during polar night, Geophysical Research Letters, 35, https://doi.org/https://doi.org/10.1029/2007GL032461, 2008.

Michaelis, J., Lüpkes, C., Schmitt, A. U., and Hartmann, J.: Modelling and parametrization of the convective flow over leads in sea ice and comparison with airborne observations, Quarterly Journal of the Royal Meteorological Society, 147, 914–943, https://doi.org/https://doi.org/10.1002/qj.3953, 2021.

Moore, G. W. K., Våge, K., Pickart, R. S., and Renfrew, I. A.: Decreasing intensity of open-ocean convection in the Greenland and Iceland seas, Nature Climate Change, 5, 877–882, https://doi.org/10.1038/nclimate2688, 2015.

Onarheim, I. H., Smedsrud, L. H., Ingvaldsen, R. B., and Nilsen, F.: Loss of sea ice during winter north of Svalbard, Tellus A: Dynamic Meteorology and Oceanography, 66, 23 933, https://doi.org/10.3402/tellusa.v66.23933, 2014.

Onarheim, I. H., Eldevik, T., Smedsrud, L. H., and Stroeve, J. C.: Seasonal and Regional Manifestation of Arctic Sea Ice Loss, Journal of Climate, 31, 4917 – 4932, https://doi.org/10.1175/JCLI-D-17-0427.1, 2018.

Schneider, T., Lüpkes, C., Dorn, W., Chechin, D., Handorf, D., Khosravi, S., Gryanik, V. M., Makhotina, I., and Rinke, A.: Sensitivity to changes in the surface-layer turbulence parameterization for stable conditions in winter: A case study with a regional climate model over the Arctic, Atmospheric Science Letters, p. e1066, https://doi.org/https://doi.org/10.1002/asl.1066, 2021.

Selyuzhenok, V., Bashmachnikov, I., Ricker, R., Vesman, A., and Bobylev, L.: Sea ice volume variability and water temperature in the Greenland Sea, The Cryosphere, 14, 477–495, https://doi.org/10.5194/tc-14-477-2020, 2020.

Shu, Q., Wang, Q., Song, Z., Qiao, F., Zhao, J., Chu, M., and Li, X.: Assessment of Sea Ice Extent in CMIP6 With Comparison to Observations and CMIP5, Geophysical Research Letters, 47, e2020GL087 965, https://doi.org/https://doi.org/10.1029/2020GL087965, 2020.

Spreen, G., Kaleschke, L., and Heygster, G.: Sea ice remote sensing using AMSR-E 89-GHz channels, Journal of Geophysical Research: Oceans, 113, https://doi.org/https://doi.org/10.1029/2005JC003384, 2008.

Stapf, J., Ehrlich, A., Jäkel, E., Lüpkes, C., and Wendisch, M.: Reassessment of shortwave surface cloud radiative forcing in the Arctic: consideration of surface-albedo–cloud interactions, Atmospheric Chemistry and Physics, 20, 9895–9914, 2020.

Steiger, J. H.: Tests for comparing elements of a correlation matrix, Psychological Bulletin, 87, 245–251, https://doi.org/10.1037/0033-2909.87.2.245, 1980.

Stroeve, J. and Notz, D.: Changing state of Arctic sea ice across all seasons, Environmental Research Letters, 13, 103 001, https://doi.org/10.1088/1748-9326/aade56, 2018.

https://doi.org/10.5194/tc-2022-185
Preprint. Discussion started: 4 October 2022

Stroeve, J., Hamilton, L. C., Bitz, C. M., and Blanchard-Wrigglesworth, E.: Predicting September sea ice: Ensemble skill of the SEARCH sea ice outlook 2008–2013, Geophysical Research Letters, 41, 2411–2418, 2014.

Stroeve, J. C., Kattsov, V., Barrett, A., Serreze, M., Pavlova, T., Holland, M., and Meier, W. N.: Trends in Arctic sea ice extent from CMIP5, CMIP3 and observations, Geophysical Research Letters, 39, 2012.

Tetzlaff, A., Lüpkes, C., Birnbaum, G., Hartmann, J., Nygård, T., and Vihma, T.: Brief Communication: Trends in sea ice extent north of Svalbard and its impact on cold air outbreaks as observed in spring 2013, The Cryosphere, 8, 1757–1762, https://doi.org/10.5194/tc-8-1757-2014, 2014.

Tetzlaff, A., Lüpkes, C., and Hartmann, J.: Aircraft-based observations of atmospheric boundary-layer modification over Arctic leads, Quarterly Journal of the Royal Meteorological Society, 141, 2839–2856, https://doi.org/https://doi.org/10.1002/qj.2568, 2015.

Wadhams, P. and Wilkinson, J.: The physical properties of sea ice in the Odden ice tongue, Deep Sea Research Part II: Topical Studies in Oceanography, 46, 1275–1300, https://doi.org/https://doi.org/10.1016/S0967-0645(99)00023-5, 1999.

Wang, Y., Bi, H., Huang, H., Liu, Y., Liu, Y., Liang, X., Fu, M., and Zhang, Z.: Satellite-observed trends in the Arctic sea ice concentration for the period 1979–2016, Journal of Oceanology and Limnology, 37, 18–37, https://doi.org/10.1007/s00343-019-7284-0, 2019.

Wendisch, M., Handorf, D., Tegen, I., Neggers, R., and Spreen, G.: Glimpsing the ins and outs of the Arctic atmospheric cauldron, Eos, 102, https://doi.org/10.1029/2021EO155959, 2021.